Supplementary Information: Stimulated cooling in non-equilibrium Bose–Einstein condensate

Ka Kit Kelvin Ho[1,‡], Vladislav Yu. Shishkov[1,‡], Mohammad Amini[1], Leonie Teresa Wrathall[1], Evgeny Mamonov[2], Darius Urbonas[3], Ioannis Georgakilas[4], Tobias M. Herkenrath[5], Michael Forster[5], Ullrich Scherf[5], Tapio Niemi[6], Päivi Törmä[2], Anton V. Zasedatelev[1]

[1] *Macroscopic Quantum Optics (MQO) Labs, Department of Applied Physics, Aalto University School of Science, FI-00076 Espoo, Finland*

[2] *Department of Applied Physics, Aalto University School of Science, FI-00076 Espoo, Finland*

[3] *IBM Research Europe – Zurich, Säumerstrasse 4, 8803 Rüschlikon, Switzerland*

[4] *Laboratory of Nano and Quantum Technologies, Paul Scherrer Institut, 5323 Villigen, Switzerland*

[5] *Macromolecular Chemistry Group and Wuppertal Center for Smart Materials and Systems (CM@S), Bergische Universitat, Wuppertal, Gauss Strasse 20, 42119 Wuppertal, Germany*

[6] *Photonics Laboratory, Physics Unit, Tampere University, Korkeakoulunkatu 3, 33720 Tampere, Finland*

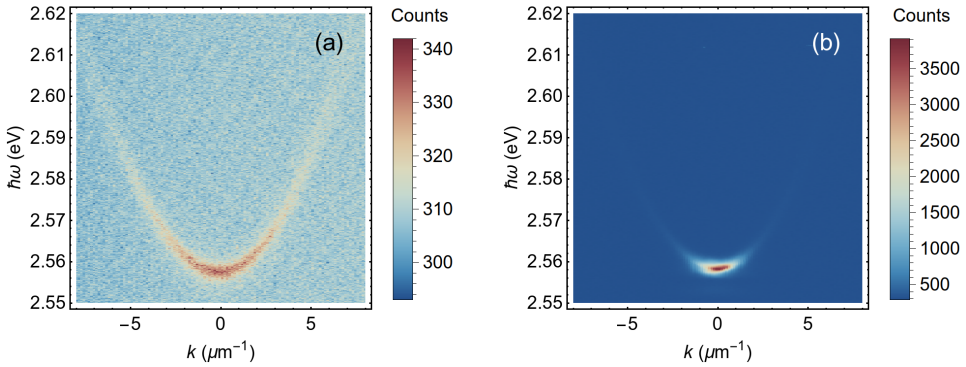

Figure S1: **Energy-momentum distribution of polaritons.** (a) Distribution at below-threshold pump power $P/P_{\text{th}} = 0.7$ and (b) at above-threshold pump power of $P/P_{\text{th}} = 1.6$. Graphs display raw data, where the vertical axis represents photon energy in electron volts and momentum in inverse microns. The color represents intensity of captured light in terms of the EMCCD photons count.

I Energy-momentum distribution of polaritons

We obtain the energy-momentum distribution of polaritons by imaging the sample emission, which occurs as light leaks out of the microcavity structure. The emission is passed through a 4f imaging system (composed of an optical telescope with a entrance lens of focal length $f_1 = 300$ and exit lens of focal length $f_2 = 150$ mm) and imaged on a spectrometery system (see methods section). The light enters the spectrometer through a 20 μm slit at the entrance of the spectrometer and onto a 1200 lines/mm grating to spectrally resolve the energy and momentum components. In Figure S1 shows photon energy-momentum distributions which maps out the polariton states when pumped at powers below and above threshold. At below threshold the distribution following a thermal distribution. At above threshold, the emission collapses around the $k = 0$ momentum and low-energy state, representing a strong momentum-space narrowing of polariton states.

II Linewidth of the high-energy fraction

The linewidth of the high-lying states broadens as pumping power increases (Figure S2). For the energy-momentum distribution at each pumping power, we restrict our analysis to a finite k-interval covering a single arm of the parabolic dispersion. At each k point of the sampled dispersion, we extract the intensity as a function of energy (along the vertical) and fit the spectrum with a Lorentzian, giving the peak energy and the linewidth (full-width half maximum) at each k point. As pumping power increases, we observe a broadening of the linewidth especially for the spectrum for larger k values. This suggests a dynamical process in which an increase in pumping power affects population dynamics.

III Single-shot realizations

We collect two sets of data, one for a pump power of $P/P_{\text{th}} = 0.7$ and another of $P/P_{\text{th}} = 1.6$, displayed in Figure S3 and S4 respectively. For each set of data, an image with a 0.75 ms

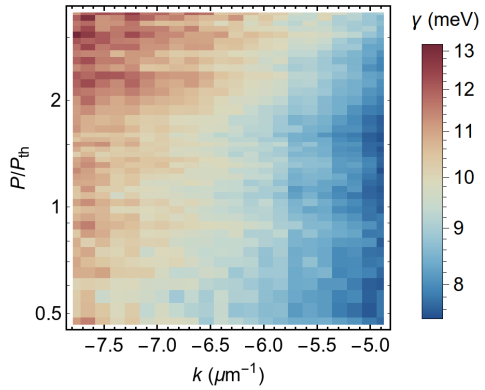

Figure S2: **Linewidth of particles in high energy fraction.** We observe that linewidth broadens as pumping power increases. The vertical axis is pumping power as a fraction of threshold power, and the horizontal axis is the k-space, limited to a subrange of the full k-space in recorded data. The linewidth γ in energy distribution for each k point is plotted in a color range.

exposure time is taken of the sample emission after the excitation of a single pulse. The timing is adjusted such that the exposure window occurs immediately after excitation but ends before the next pulse. This ensures that the captured image pertains to the excitation by a single pulse. The pulse power is also captured by a calibrated photodiode (see Methods). The recorded signal is a Lorentzian peak which is the convolution between the power impinging on the photodiode and the detector response. This allows us to correlate the captured image and excitation power. We perform 100 of such correlated measurements for each of the two pumping power. We average the realizations to obtain a single momentum-space image corresponding to the excitation power.

IV Fit of the particle distribution with one Bose–Einstein distribution

To fit the distributions of the particles over energies with Bose–Einstein distribution, we transform the data, presented in Figure 3a of the main text, according to

$$N_{\mathrm{pol}} \to \ln\left(\frac{g}{N_{\mathrm{pol}}} + 1\right). \tag{S1}$$

This transformation results in a linear function of energy in the case of pure Bose–Einstein distribution. The transformation for experimentally measured distribution of the particles shows that a single Bose–Einstein distribution fit is insufficient to describe the full population dynamics, which is evident from Figure S5. Instead, the particles split in two fractions: high-energy fraction and low-energy fraction, following linear dependencies (Fig. S5). These two fractions follow Bose–Einstein distribution, albeit their respective temperatures and chemical potentials are different. We perform a linear regression [1] for the transformed data to (Fig. S5) to extract temperatures and chemical potentials of the low-energy fraction and high-energy fraction of the particles depending on the pump (see Table 1 and 2).

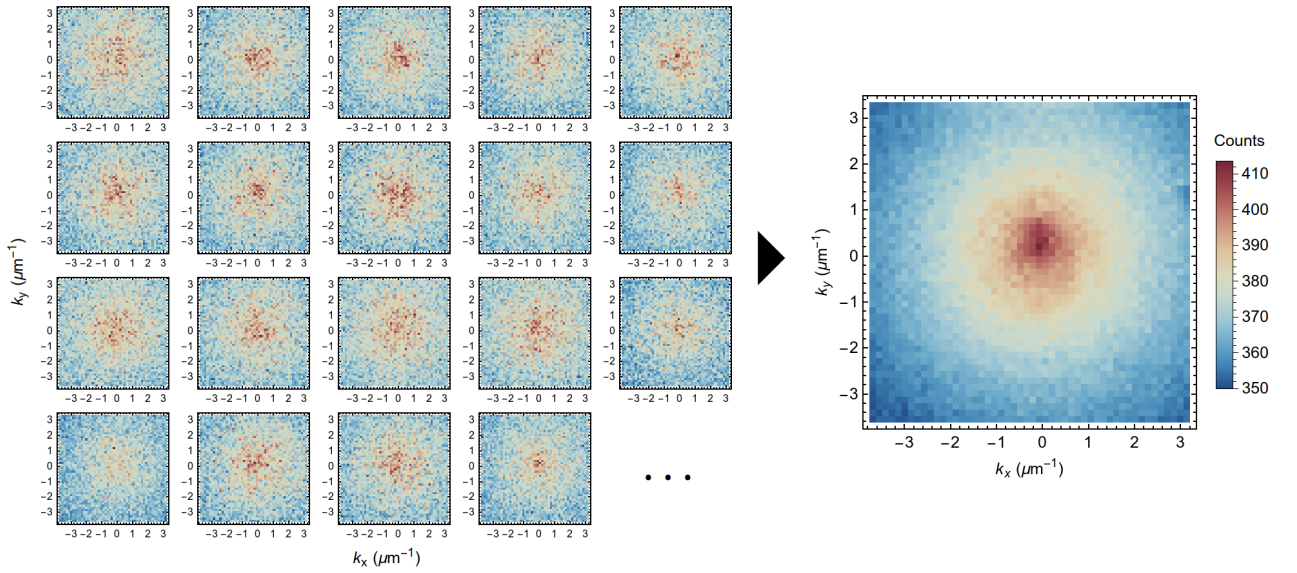

Figure S3: **Single shot realizations below threshold.** Momentum space image for $P/P_{\text{th}} = 0.7$. Left is a collection of individual single shot image, in which the momentum space image is immediately captured after the sample is excited by a single pulse. Right is the average of the recorded single-shot realizations. The size of the sample is 100 shots.

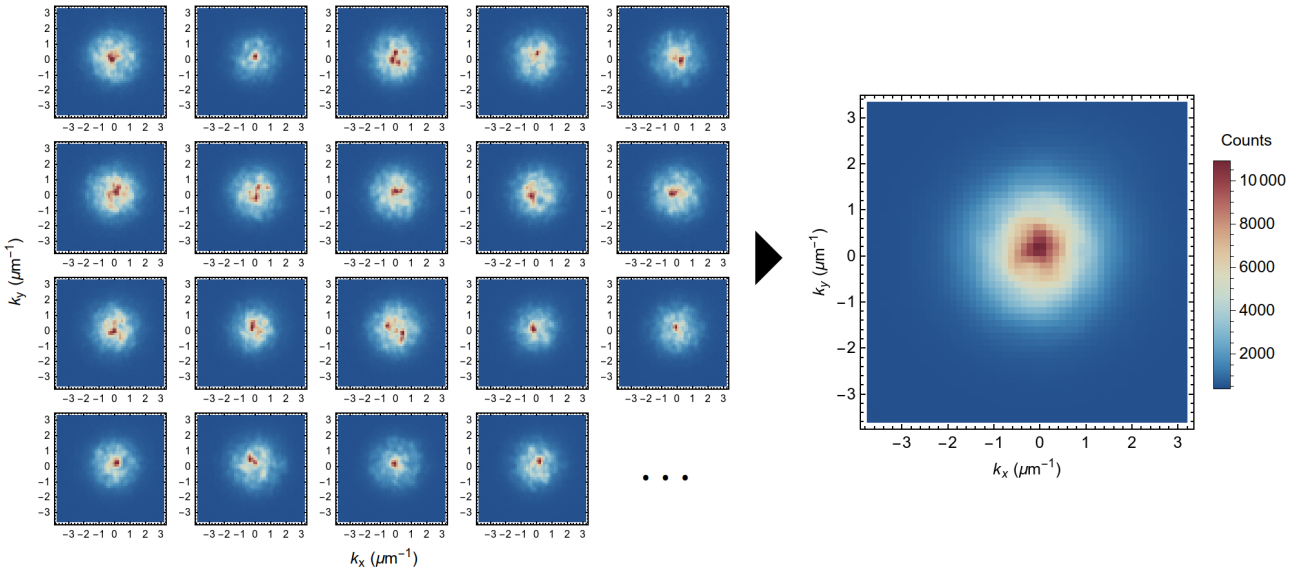

Figure S4: **Single shot realizations above threshold.** Momentum space image for $P/P_{\text{th}} = 1.6$. Left is a collection of individual single shot image, in which the momentum space image is immediately captured after the sample is excited by a single pulse. Right is the average of the recorded single-shot realizations. The size of the sample is 100 shots.

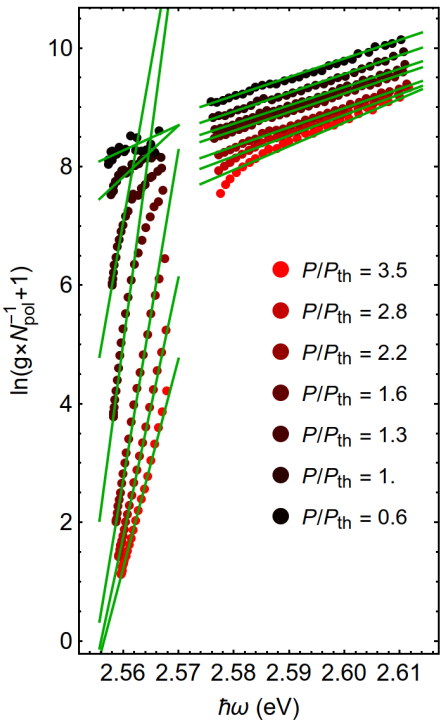

Figure S5: **Logarithmic representation of population data.** We plot the data presented in Figure 3 of the main text in logarithmic form (Eq. (S1)) to better illustrate how the population follows a Bose–Einstein population. Furthermore, it can be clearly seen that the high and low-energy fraction follows their own Bose–Einstein distribution with a different temperature and chemical potential. Solid lines shows the results of the linear regression for the low-energy and high-energy fractions of the particles.

P/P_{th}	T_{L} (meV)	μ_{L} (meV)
3.53	2.831 ± 0.022	-3.178 ± 0.036
3.29	2.679 ± 0.021	-3.184 ± 0.037
3.18	2.552 ± 0.022	-3.129 ± 0.041
3.06	2.485 ± 0.024	-3.120 ± 0.046
2.82	2.299 ± 0.021	-3.163 ± 0.043
2.71	2.169 ± 0.018	-3.234 ± 0.039
2.59	2.113 ± 0.016	-3.379 ± 0.038
2.35	1.960 ± 0.023	-3.77 ± 0.06
2.26	1.797 ± 0.020	-3.68 ± 0.05
2.12	1.646 ± 0.024	-3.73 ± 0.06
1.88	1.448 ± 0.032	-4.219 ± 0.010
1.76	1.406 ± 0.042	-4.794 ± 0.15
1.65	1.436 ± 0.046	-5.53 ± 0.18
1.60	1.42 ± 0.05	-6.02 ± 0.23
1.56	1.41 ± 0.06	-6.46 ± 0.26
1.46	1.54 ± 0.07	-7.83 ± 0.37
1.41	1.61 ± 0.07	-8.68 ± 0.41
1.32	1.89 ± 0.09	-11.4 ± 0.5
1.22	1.99 ± 0.11	-13.1 ± 0.7
1.18	2.10 ± 0.12	-14.5 ± 0.8
1.08	2.18 ± 0.26	-15.82 ± 1.9
1.04	2.6 ± 0.5	-19.8 ± 3.9
0.99	11.5 ± 0.8	-88 ± 6
0.89	11.9 ± 0.7	-94 ± 5
0.80	19.0 ± 2.1	-152 ± 17
0.71	20.1 ± 2.3	-164 ± 19
0.61	23.5 ± 3.4	-192 ± 28
0.52	17.9 ± 2.0	-150 ± 16

Table 1: **Temperature and chemical potential for low-energy fraction.** The extracted temperature, T_{L}, and chemical potential, μ_{L}, with their standard errors obtained from the linear regression of $\ln\left(g{N_{\mathrm{pol}}}^{-1}+1\right)$ for low-energy fraction of the particles (see Fig. S5).

P/P_{th}	T_{H} (meV)	μ_{H} (meV)
3.53	25.03 ± 0.49	-178.6 ± 3.6
3.29	25.8 ± 0.5	-186.8 ± 3.9
3.18	25.6 ± 0.5	-184.4 ± 3.7
3.06	27.87 ± 0.40	-205.1 ± 3.0
2.82	27.97 ± 0.34	-208.4 ± 2.6
2.71	27.58 ± 0.44	-205.9 ± 3.3
2.59	28.74 ± 0.37	-216.5 ± 2.8
2.35	30.87 ± 0.40	-234.9 ± 3.1
2.24	30.84 ± 0.39	-236.0 ± 3.0
2.12	30.81 ± 0.47	-237.5 ± 3.7
1.88	31.37 ± 0.48	-245.1 ± 3.8
1.76	30.88 ± 0.43	-242.5 ± 3.4
1.65	31.86 ± 0.40	-252.4 ± 3.2
1.60	30.52 ± 0.49	-241.8 ± 3.9
1.55	31.10 ± 0.49	-247.1 ± 3.9
1.46	31.2 ± 0.6	-248.2 ± 4.5
1.41	30.8 ± 0.7	-245 ± 5
1.32	32.3 ± 0.6	-260.2 ± 4.8
1.22	32.1 ± 0.5	-260.1 ± 4.3
1.18	32.3 ± 0.5	-262.8 ± 4.3
1.08	31.9 ± 0.6	-261.4 ± 4.8
1.04	33.3 ± 0.6	-274 ± 5
0.99	31.6 ± 0.7	-260 ± 6
0.89	34.1 ± 0.6	-283 ± 5
0.80	32.5 ± 0.7	-271 ± 6
0.71	31.8 ± 0.8	-267 ± 7
0.61	31.9 ± 0.7	-271 ± 6
0.52	32.0 ± 0.8	-275 ± 7

Table 2: **Temperature and chemical potential for high-energy fraction.** The extracted temperature, T_{H}, and chemical potential, μ_{H}, with their standard errors obtained from the linear regression of $\ln\left(g{N_{\mathrm{pol}}}^{-1}+1\right)$ for low-energy fraction of the particles (see Fig. S5).

V Theoretical model of BEC in NVT-ensemble

The partition function of an ideal 2D Bose gas with parabolic dispersion, Z_N, above the condensation threshold is $Z_N \approx Z_\infty (1 - G_{2D}/N)$ [2], where G_{2D} is the number of states in the range $\{\hbar\omega_{\rm gs}, \hbar\omega_{\rm gs} + k_B T\}$ with $\hbar\omega_{\rm gs}$ being the energy of the ground state, and $Z_\infty = \exp[G_{2D}\zeta(2)]$ with $\zeta(x)$ being Riemann zeta function. The chemical potential μ in NVT-ensemble is $\mu = -k_B T \ln(Z_{N+1}/Z_N)$ [3], therefore above the condensation threshold

$$\mu \approx -k_B T \frac{G_{2D}}{N^2}. \tag{S2}$$

Given that $G_{2D} \propto T$ [2], we obtain $\mu \propto -T^2$ for ideal 2D Bose gas with parabolic dispersion above the condensation threshold.

The second-order cross-correlation function between the ground state and excited state with wave vector $\mathbf{k}$ for an ideal Bose gas in NVT-ensemble is $g^{(2)}_{\mathbf{k}=\mathbf{0}\mathbf{k}} = \langle \hat{n}_{\mathbf{k}=\mathbf{0}} \hat{n}_{\mathbf{k}} \rangle_N / \langle \hat{n}_{\mathbf{k}=\mathbf{0}} \rangle_N \langle \hat{n}_{\mathbf{k}} \rangle_N$, where subscript N denotes the total number of particles in the ensemble. From the theory of an ideal 2D Bose gas with parabolic dispersion in NVT-ensemble [2], it follows $\langle \hat{n}_{\mathbf{k}=\mathbf{0}} \hat{n}_{\mathbf{k}} \rangle_N = \langle \hat{n}_{\mathbf{k}} \rangle_\infty \langle \hat{n}_{\mathbf{k}=\mathbf{0}} \rangle_N - (1 + \langle \hat{n}_{\mathbf{k}} \rangle_\infty) \langle \hat{n}_{\mathbf{k}} \rangle_N$, where $\langle \hat{n}_{\mathbf{k}} \rangle_\infty = (\exp(\hbar\omega_{\mathbf{k}}/k_B T) - 1)^{-1}$. Above the condensation threshold $\langle \hat{n}_{\mathbf{k}=\mathbf{0}} \rangle_N \approx N - G_{2D} \ln N$ and $\langle \hat{n}_{\mathbf{k}} \rangle_N \approx \langle \hat{n}_{\mathbf{k}} \rangle_\infty - \frac{G_{2D}}{N^2} e^{-\hbar\omega_{\mathbf{k}}/k_B T} \langle \hat{n}_{\mathbf{k}} \rangle^2_\infty$. Therefore

$$g^{(2)}_{\mathbf{k}=\mathbf{0}\mathbf{k}} \approx 1 + \frac{\langle \hat{n}_{\mathbf{k}} \rangle_\infty}{N} \left(\frac{G_{2D}}{N} e^{-\hbar\omega_{\mathbf{k}}/k_B T} - 1 \right) < 1 \tag{S3}$$

Thus, the statistical theory for ideal 2D Bose gas with quadratic dispersion in NVT-ensemble predicts anti-correlations of the particles in the ground and excited states, $\langle \hat{n}_{\mathbf{k}=\mathbf{0}} \hat{n}_{\mathbf{k}} \rangle_N < \langle \hat{n}_{\mathbf{k}=\mathbf{0}} \rangle_N \langle \hat{n}_{\mathbf{k}} \rangle_N$, above the condensation threshold. These anti-correlations has been also predicted theoretically for non-equilibrium ideal Bose gas in the fast thermalization limit [4].

References

[1] James, G., Witten, D., Hastie, T. & Tibshirani, R. *An introduction to statistical learning with applications in R* (Springer, 2013).

[2] Shishkov, V. Y., Andrianov, E. S. & Lozovik, Y. E. Analytical framework for non-equilibrium phase transition to Bose–Einstein condensate. *Quantum* **6**, 719 (2022). URL https://doi.org/10.22331/q-2022-05-24-719.

[3] Kubo, R. *Statistical mechanics: an advanced course with problems and solutions* (North-Holland, Amsterdam, 1988).

[4] Shishkov, V. Y., Andrianov, E. S., Zasedatelev, A. V., Lagoudakis, P. G. & Lozovik, Y. E. Exact analytical solution for the density matrix of a nonequilibrium polariton bose-einstein condensate. *Phys. Rev. Lett.* **128**, 065301 (2022). URL https://link.aps.org/doi/10.1103/PhysRevLett.128.065301.